INTERNATIONAL JOURNAL OF CLIMATOLOGY
Int. J. Climatol. (2016)
Published online in Wiley Online Library
(wileyonlinelibrary.com) DOI: 10.1002/joc.4658

RMetS
Royal Meteorological Society

The warm pool variability of the tropical northeast Pacific

Vasubandhu Misra,[a,b,c]* Danielle Groenen,[a,b] Amit Bharadwaj[a] and Akhilesh Mishra[a]

[a] *Center for Ocean-Atmospheric Prediction Studies, Florida State University, Tallahassee, FL, USA*
[b] *Department of Earth, Ocean and Atmospheric Science, Florida State University, Tallahassee, FL, USA*
[c] *Florida Climate Institute, Florida State University, Tallahassee, FL, USA*

ABSTRACT: The Eastern Pacific warm pool (EPWP) defined by the area enclosed within the 28.5 °C isotherm is examined for its seasonal cycle and interannual variability. The study characterizes the EPWP by its area and objectively defined onset, demise, and length of its seasonality. The onset of the EPWP season is defined by the day when the daily anomaly of the area of EPWP exceeds its climatological annual mean. Similarly, the demise of the EPWP season is defined when the daily anomaly of the area of the EPWP falls below its climatological annual mean, after the onset date is detected. We show that the seasonal evolution of the EPWP has a strong asymmetry, with the climatological peak of the EPWP area occurring approximately 41 days from the onset while the demise of the season occurs after nearly 106 days from the climatological peak. The EPWP is part of a larger Western Hemisphere warm pool (WHWP) that extends into the Intra-Americas Seas and parts of the tropical northwest Atlantic Ocean. This study finds that the EPWP is weakly related to the Atlantic counterpart of the WHWP. This is partly due to the fact that the EPWP season precedes the seasonal peak of the warm pool in the Atlantic by several months and the size of the former is much smaller than the latter; therefore, the EPWP does not have a strong remote forcing on the Atlantic warm pool. The interannual variability of the area of EPWP is closely related to the El Niño and the Southern Oscillation (ENSO) variations in the equatorial Pacific with large (small) EPWP years associated with warm (cold) ENSO years.

KEY WORDS warm pool; ENSO; monsoon

Received 29 May 2015; Revised 27 October 2015; Accepted 22 December 2015

1. Introduction

The Eastern Pacific warm pool (EPWP) is a part of the Western Hemisphere warm pool (WHWP), which was first identified by Wang and Enfield (2001) to be the largest body of warm water (≥28.5 °C) in the Western Hemisphere. They showed that WHWP contributes significantly to the large-scale Hadley-type overturning circulation centred over the tropical western Atlantic Ocean during boreal summer and fall seasons. The larger Atlantic counterpart of the WHWP, which is called the Atlantic Warm Pool (AWP), appears in early boreal summer and is preceded by the appearance of the EPWP. The aim of this study is to analyse the seasonal to interannual variability of the EPWP and diagnose its remote teleconnections.

A number of studies have reviewed the EPWP region for its surface and sub-surface oceanic features [e.g. Wyrtki, 1964, 1965, 1966, 1967; Fiedler, 2002; Xie *et al.*, 2005; Kessler, 2006; Willett *et al.*, 2006; Karnauskas and Busalacchi, 2009a, 2009b (hereafter KB9a,b)]. These studies have shown that the EPWP circumscribes a relatively smaller but important oceanographic feature called the Costa Rica Dome, which manifests in the shoaling of the thermocline centred around 9°N and 90°W. The EPWP is also recognized to fuel one of the important atmospheric convection centres of our planet, which is the northward extension of the eastern Pacific Inter-Tropical Convergence Zone (ITCZ; Mitchell and Wallace, 1992; Wang and Enfield, 2003; Xie *et al.*, 2005; Amador *et al.*, 2006; Wang and Fiedler, 2006). The surface winds in the EPWP tend to be relatively weak (Raymond *et al.*, 2004). But episodic intense deep convective events are related to strong wind events, which is a result of the strong turbulent surface fluxes generated by the strong winds (Raymond *et al.*, 2003). The EPWP region is also known for its intense cyclonic activity (Banichevich and Lizano, 1998; Maloney and Hartmann, 2000; Wood and Ritchie, 2013; Crosbie and Serra, 2015; Jien *et al.*, 2015). A significant fraction of these eastern Pacific tropical cyclones are shown to contribute rainfall over the southwestern United States and Mexico (Ritchie *et al.*, 2010).

Several studies have shown that the interannual variability of sea-surface temperature (SST) in the EPWP is highly correlated to El Niño and Southern Oscillation (ENSO) variations (Wang and Enfield, 2003; Xie *et al.*, 2005; KB9a). KB9a indicate that this is a consequence of shortwave flux anomalies over the EPWP that arises in response to the modulation of eastern Pacific ITCZ by ENSO. They further indicate that the poleward ocean heat transport from the equatorial latitudes was insufficient to explain EPWP's observed interannual variability.

* Correspondence to: V. Misra, Center for Ocean-Atmospheric Prediction Studies, Florida State University, 2000 Levy Avenue, Suite 292, Tallahassee, FL 32306, USA. E-mail: vmisra@fsu.edu

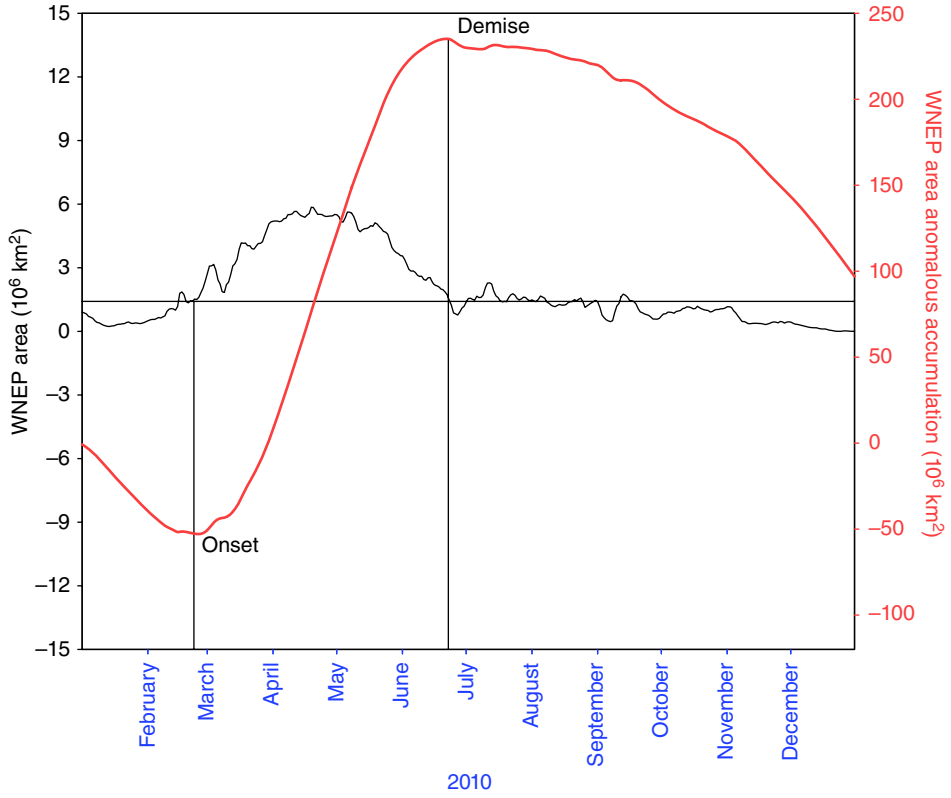

Figure 1. The time series of daily cumulative anomalies (in red) and the daily anomalies of the EPWP area for the year 2010. The date of onset and demise of the EPWP is marked.

In this study, we examine the EPWP variability and its potential teleconnections by investigating the variations in the area of the EPWP and the uniquely defined onset and demise dates of the EPWP season.

2. Methodology and data sets

As previously noted, the area of the EPWP is computed as the area enclosed by the 28.5 °C isotherm. This particular isotherm was so chosen because it encompasses the WHWP that has shown to have a strong bearing on the regional climate of North America (Wang and Enfield, 2003; Wang *et al.*, 2007). Because of the strong seasonality of the appearance of this isotherm in the tropical northeastern Pacific Ocean, we make use of the methodology from previous studies (Liebmann *et al.*, 2007; Misra *et al.*, 2014) to objectively define the onset, seasonal peak, demise, and length of the EPWP season. Variables that depict a very strong seasonal cycle exhibit a sharp change in their daily cumulative anomalies (DCA; computed with respect to its climatological annual mean) at the time of their onset and demise (Figure 1). The DCA for the area of the EPWP accumulated to the mth day of the kth year is given by

$$\mathrm{DCA}_k(m) = \sum_{i=1}^{m} \left\{A'_k(i)\right\} \qquad (1)$$

where $A'_k(i)$ is the daily anomalous area of the EPWP for the ith day of the kth year.

For example, in Figure 1 we show the time series of the DCA of the area of the EPWP for the year 2010 that had its onset date on the 56th Julian day and demise date on the 173rd Julian day of the EPWP seasonal cycle. The day of the onset of the EPWP season in Figure 1 is determined by the day after the DCA reaches its minimum. Similarly, the demise of the EPWP season is determined by the day after the DCA reaches its maximum. Alternatively, in this case the onset (demise) date also translates to the date when daily anomalies of the area of the EPWP exceed (fall below) the climatological annual mean. The day of the seasonal peak of EPWP is determined by the day when the area of the EPWP is the largest between the onset and demise dates.

KB9a defined EPWP as the area average SST over a fixed area off the western coast of Central America that roughly circumscribed the 28 °C isotherm in the annual mean climatological SST (cf. Figure 1). This definition of the EPWP in KB9a is quite different from the one used in this paper. We compare these definitions of EPWP along with the area average SST enclosed within the 28.5 °C isotherm in Figure 2 and Table 1. We notice in Figure 2 that all three metrics of EPWP display a significant linear trend that passes the Mann–Kendall test at 5% significance level (Sneyers, 1990). Further, we also see that the definition of EPWP of this paper and that of KB9a correlates at 0.88, which suggests that these definitions capture similar interannual variations. However, the variability of the SST within the 28.5 °C isotherm (Figure 2(b)) is relatively

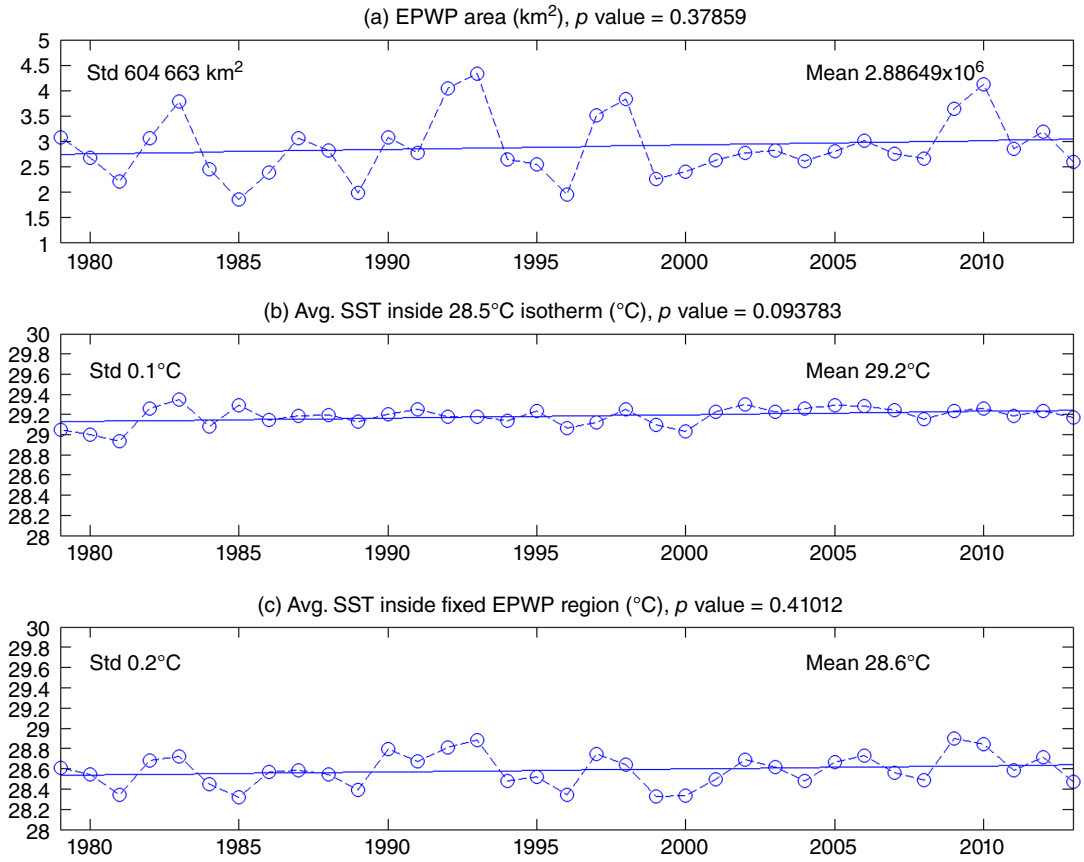

Figure 2. Time series of the seasonal mean (a) area of the EPWP as defined by the area of the 28.5 °C isotherm, (b) SST enclosed within the 28.5 °C isotherm, and (c) SST inside a fixed EPWP region from KB9a. The seasonal mean for each year for all three time series is computed between the time of onset and demise as delineated in Figure 1 and associated discussion in the text. The standard deviation and the mean values of the three time series are indicated in each of the panel. The slope of the linear fit is (a) 0.011509×10^6 km^2 year^{-1}, (b) 0.0034 °C year^{-1}, and (c) 0.0030 °C year^{-1}. In all three time series, the indicated p values suggest that the slope exceeds the 5% significance level according to Mann–Kendall test.

weak, and its correlations with either the seasonal area of the EPWP (Figure 2(a)) or the EPWP definition of KB9a (Figure 2(c)) are comparatively weak (Table 1).

The SSTs used in this study are from the NOAA Optimally Interpolated daily values version 2 (Reynolds *et al.*, 2007) available at 0.25° × 0.25° resolution globally. The rainfall data analysed for this work come from the Climate Prediction Center (CPC) Unified Gauge-Based Analysis of Global Daily Precipitation on a 0.5° grid (Chen *et al.*, 2008). The upper air variables are from the National Centers for Environmental Prediction (NCEP) Climate Forecast System Reanalysis (Saha *et al.*, 2010). We have also used the daily air-sea fluxes at 1° grid size from Yu *et al.* (2008). The time period of the observational analysis conducted in this paper is for a 35-year period from 1979 to 2013. However, the surface fluxes were available till only 2009.

3. Results

3.1. Climatology

The climatological mean SST at the time of the onset of the EPWP season is shown in Figure 3(a). At this time of the seasonal cycle of the EPWP (March 22; Table 2), SSTs that are warmer than 28.5 °C appear in three small patches. One patch is off the coast of Costa Rica and just south of the Gulf of Papagayo, another is to the north while the third patch of warm water ≥28.5 °C is to the south of the Gulf of Tehuantepec. This pattern of three incoherent patches of very warm SSTs is largely due to the strong gap winds coming off the coast, caused by easterly trade winds coming through the gaps in the Sierra Madre de Chiapas and creating large areas of upwelling (Small *et al.*, 2007). The key feature in Figure 3(a) is the larger and far more coherent area of 28 °C SST (shaded in light blue) extending further westward to 120°W, which underlies these three onset patches of the EPWP. The area of the 28 °C isotherm in the EPWP is likely influencing large-scale dynamics more than the spatially incoherent, small patches of SSTs >28.5 °C at the time of the onset date. The signature of the double ITCZ with relatively warm SSTs (≥27 °C) on either side of the cold eastern equatorial Pacific is also clearly observed in this composite (Figure 3(a)). At the peak of the EPWP season [Figure 3(b); May 2 (Table 2)], the EPWP extends from the Central American coast to about 125°W with an area of even warmer SSTs (≥29 °C) extending to nearly 110°W from the Central American coast. It is important to note that the AWP has still not appeared at the peak of the EPWP season. At the time

Table 1. Linear correlations of the various seasonal measures of EPWP variability.

	EPWP area represented by area of 28.5 °C isotherm (Figure 2(a))	Seasonal mean SST anomalies inside the 28.5 °C isotherm (Figure 2(b))	Seasonal mean SST inside a fixed region of EPWP defined in KB9a (Figure 2(c))
Linear correlation	**0.35 (0.32)**	**0.88 (0.88)**	**0.48 (0.45)**

The correlations after the linear trend of the corresponding time series removed are indicated in brackets. Bold values indicate that they are significant at 10% significance level according to *t*-test.

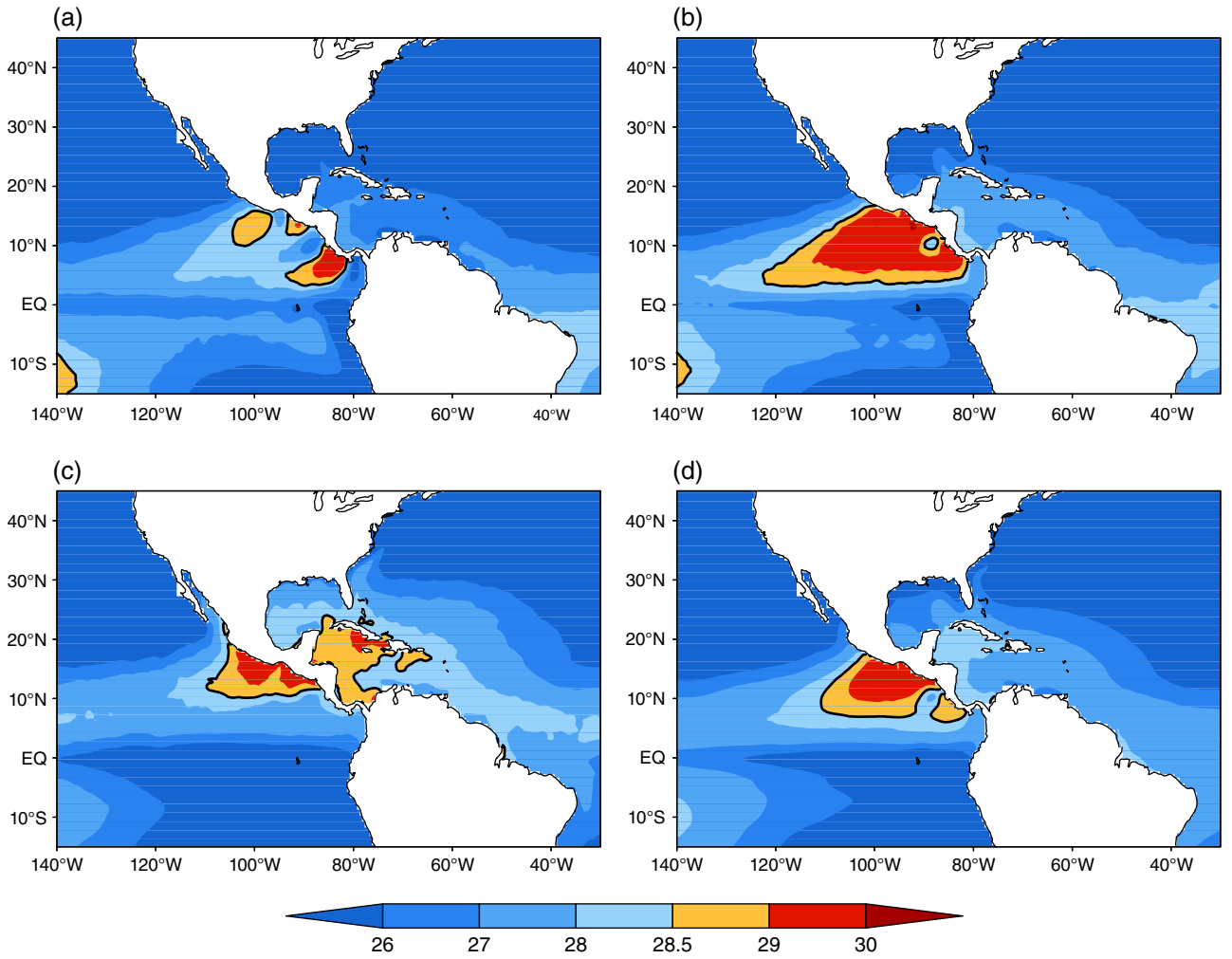

Figure 3. The climatological mean SSTs (°C) at time of (a) onset, (b) peak, and (c) demise of the warm pool in the tropical northeast Pacific, and (d) the climatological mean SSTs between onset (March 22) and demise (August 16) dates of the WNEP.

of the demise of the EPWP season [Figure 3(c); August 16 (Table 2)], the warm pool has significantly receded to the coast from its seasonal peak. But unlike the time of the onset (Figure 3(a)), the area of the EPWP is far more coherent at the time of demise. Furthermore, there is a clear development of the AWP at the time of demise of the EPWP (Figure 3(c)). The seasonal mean area of the EPWP (Figure 3(d)) computed as the mean of the area enclosed by the 28.5 °C isotherm between the dates of onset and demise of each year is shown to extend from the Gulf of Papagayo to the south and to the coast of Acapulco in southern Mexico in the north, with the westward extent to around 110°W. A smaller coherent patch of warm pool (≥28.5 °C) is also formed in the Gulf of Chiriqui, south of the Gulf of Papagayo. Overall, the seasonal mean EPWP (Figure 3(d)) is enclosed within a larger coherent ≥28.0 °C isotherm. It may be noted again that the seasonal mean EPWP does not show the AWP (Figure 3(d)). However, it is important to note that the climatological length of the EPWP season is about 147 days (Table 2), which is relatively long, and stretches over nearly 5 months. From Table 2, it is also clear that the seasonal evolution of the EPWP is quite asymmetric in terms of onset date and demise date. The climatological seasonal peak of the EPWP occurs in about 41 days from the onset date. The demise of the EPWP occurs much more slowly, after 106 days from the climatological peak of the season.

Table 2. Average dates of onset, peak, and demise of the warm pool in the tropical northeast Pacific.

	Climatology (Julian day)	El Niño composite	La Niña composite
Onset	81 (March 22)	83 (March 24)	70 (March 11)
Peak	122 (May 2)	120 (May 1)	124 (May 4)
Demise	228 (August 16)	281 (October 7)	198 (July 17)

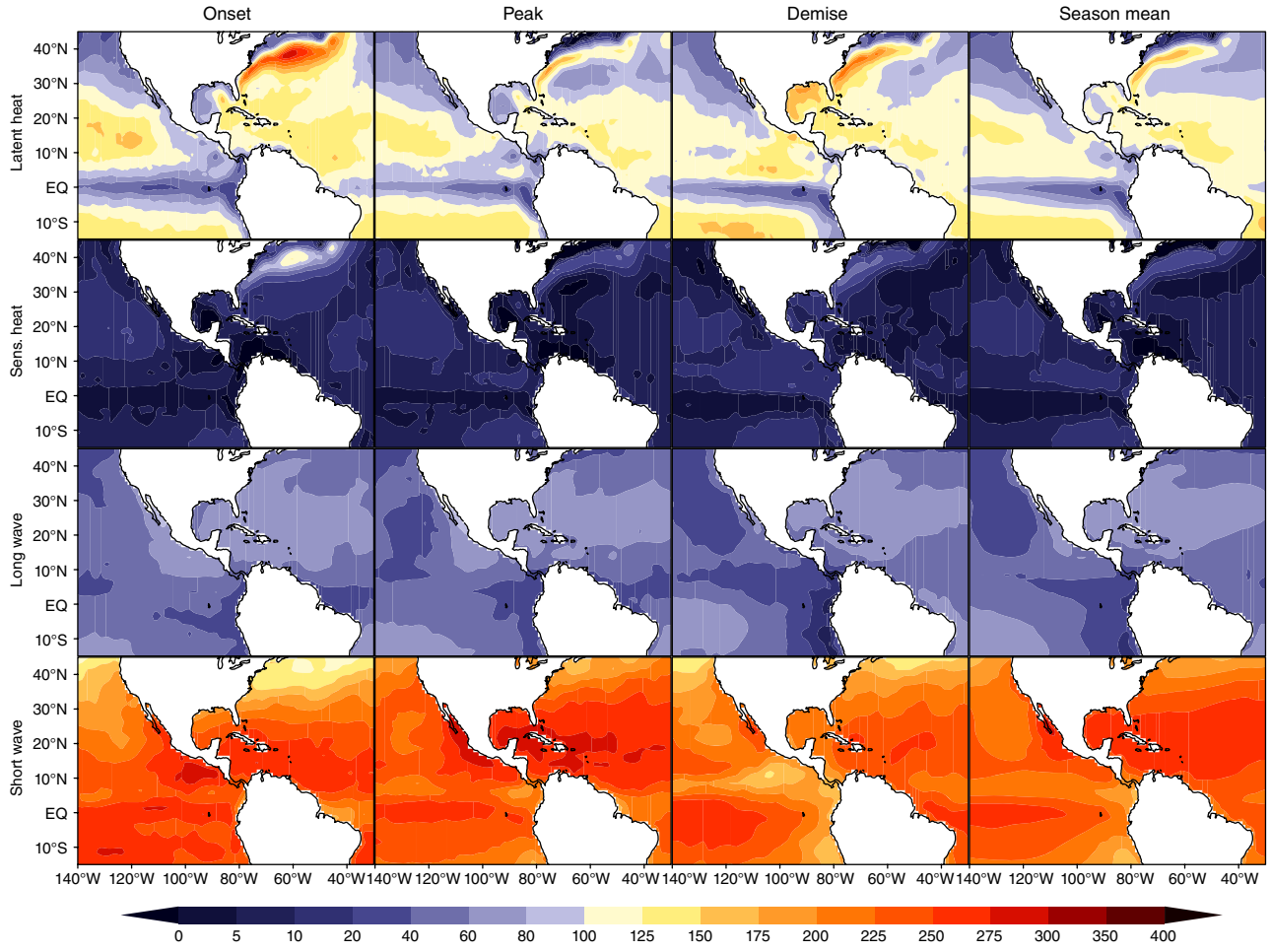

Figure 4. The climatological mean surface (top row) latent heat flux, (second row) sensible heat flux, (third row) net longwave flux, and (bottom row) net shortwave flux at time of onset, seasonal peak, demise, and seasonal mean (from left to right). The units are in W m^{-2}.

This asymmetry can be explained in the meridional migration of the eastern Pacific ITCZ (cf Figure 3 in Hastenrath, 2002). Hastenrath (2002) clearly indicates that the latitude of wind confluence of the eastern Pacific ITCZ exhibits a large meridional migration between February and May of each year, and thereafter the meridional movement is relatively very weak until around October. This asymmetry of the atmospheric ITCZ in turn affects the SSTs through the wind-evaporation-SST feedback (Xie and Philander, 1994) leading to the asymmetry in the seasonal cycle of the EPWP. Lee *et al.* (2007) also show in their study that the seasonal growth of the EPWP is dominated by the clear-sky shortwave radiation flux in the boreal spring season and its associated reduction with the increased cloud cover from the northward propagation of the ITCZ results in its demise. This seasonal cycle of the EPWP coincides with the seasonal cycle of the Costa Rica dome and the meridional migration of the ITCZ (not shown; Fiedler, 2002).

A composite of the surface fluxes at time of onset, seasonal peak, demise of EPWP is shown along with the seasonal mean in Figure 4. The figure shows that the seasonal cycle of the EPWP is also characterized by distinct changes in the seasonal cycle of the surface fluxes in the region. For example, at the time of the onset of the EPWP, the latent heat fluxes are larger on the western edges of the EPWP while near the western coast of Central America they are comparatively weaker. But by the time of the demise of the EPWP, the latent heat flux becomes large till the western coast of Central America. The variations in the sensible heat flux are much weaker compared to the latent heat flux, although they show an opposite pattern, with western coast of Central America displaying more sensible heat at time of onset than at time of demise of

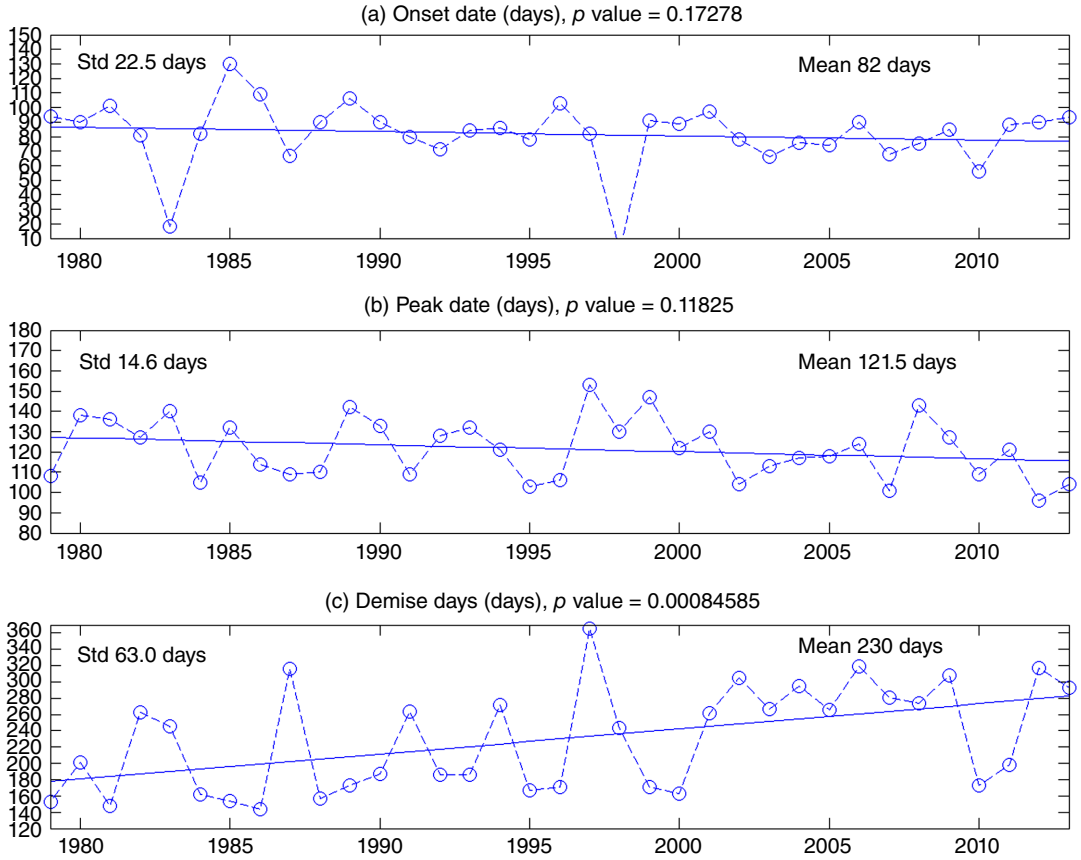

Figure 5. Same as Figure 2 but for time series of the time of (a) onset (Julian day), (b) peak (Julian day), (c) demise (Julian day), and (d) total area of the warm of pool ($\times 10^6$ km^2) in the tropical northeast Pacific. The slope of the linear trends is (a) −0.29 days year^{-1}, (b) −0.34 days year^{-1}, and (c) 3.1 days year^{-1}.

Table 3. Linear correlations of the variants of EPWP.

	Onset date of the warm pool in the tropical northeast Pacific (EPWP)	Demise date of the EPWP	Length of the EPWP season	Seasonal average of the area of the EPWP
Onset date of EPWP	**1.0**	−0.29 (−0.05)	**−0.56 (−0.56)**	**−0.66 (−0.64)**
Demise date of EPWP	−0.29 (−0.05)	**1.0**	**0.96 (0.94)**	0.28 (0.24)
Length of the EPWP	**−0.56 (−0.56)**	**0.96**	**1.0**	**0.45 (0.43)**

The correlation in brackets is obtained after the corresponding linear trend is removed. (Statistically significant values at 90% confidence interval according to *t*-test is in bold.)

EPWP. The net surface radiative fluxes are dominated by the shortwave fluxes. The shortwave fluxes over the EPWP regions are strongest at seasonal peak and weakest at time of demise. The downwelling net longwave radiative flux, albeit nearly five times smaller than the shortwave flux, is largest (smallest) over the EPWP at time of onset (demise).

3.2. Interannual variations

ENSO variations have an influence on the seasonal cycle of the EPWP. For example, the anomalously late demise of the EPWP season in 1997 (Figure 5(c)) and anomalously early onset of the EPWP season in 1998 (Figure 5(a)) are a transition from 1 year to the next without a seasonal break. In this particular year, the EPWP was defined throughout the year, when ENSO conditions persisted for nearly a year and 4 months. Similarly, in relatively strong but weaker than 1997–1998 ENSO years like 1982–1983 and 1987–1988, we see a similar pattern of late demise (Figure 5(c)) from the previous year to an early onset (Figure 5(a)) of EPWP in the following year but with a seasonal break when the EPWP is undefined. The composite dates for onset, seasonal peak, and demise of the EPWP for warm and cold ENSO years are listed in Table 1. These composites of ENSO between 1979 and 2013 are based on SST anomalies exceeding a 0.5 °C anomaly for any of the four overlapping 3-month seasons starting from April–May–June (AMJ) season of the year (following http://www.cpcp.ncep.noaa.gov/products/analysis_monitoring/ensostuff/ensoyears.shtml). This criterion for defining the composites was chosen so that steady ENSO

Table 4. Linear correlations between EPWP and AWP.

	Onset date of the warm pool in the tropical northeast Pacific (EPWP)	Demise date of the EPWP	Length of the EPWP season	Seasonal average of the area of the EPWP
Onset date of AWP	0.37 (0.35)	−0.16 (−0.06)	−0.25 (−0.07)	−0.36 (−0.30)
Demise date of the AWP	−0.24 (−0.21)	**0.46** (0.21)	**0.48** (0.25)	0.23 (0.18)
Length of the AWP	−0.35 (−0.34)	0.35 (0.07)	**0.41** (0.18)	0.33 (0.29)
Seasonal average of the area of the AWP	−0.27 (−0.21)	0.33 (0.07)	0.37 (0.14)	0.17 (0.07)

We have also indicated correlation in brackets after the corresponding linear trends are removed both in EPWP and AWP variants. (Statistically significant values at 90% confidence interval is in bold.)

forcing is present for the majority of the length of the EPWP season. These composites comprise of nine such warm and cold ENSO years. It is apparent from Table 2 that the demise date of the EPWP is most sensitive to ENSO followed by that of the onset date. This is also apparent in the variability of the time series of the dates of onset, seasonal peak, and demise of the EPWP (Figure 5). The seasonal peak date of the EPWP is the least sensitive to ENSO variations (Table 2).

It is also apparent from Figure 5 that the onset and peak dates of the EPWP show a strong linear trend (which passes the Mann–Kendall significance test at 5% significance level). The demise date of the EPWP despite displaying a comparatively large slope of the linear trend (as large as 3.1 days year^{-1}) however fails the significance test because of the strong variability it carries. But as in Misra *et al.* (2014), we are sceptical of removing this apparent trend from a relatively short record of just 35 years. Moreover, the Pacific basin displays robust decadal variations ranging with time periods of 15–50 years (Minobe, 1997; Zhang *et al.*, 1997), which can easily appear as a linear trend in this type of data record length. In any case, even after removing these trends, the correlations indicated in Tables 3 and 4 did not change significantly between those variables whose relationships are emphasized in this study.

The composite mean over the length of the EPWP season for 10 years with the smallest and largest area of the EPWP is shown in Figure 6(a) and (b), respectively. The difference in the area of the EPWP between the two composites is approximately 10% of the mean area of the EPWP. The SST difference field between Figure 6(b) and (a) clearly indicates the warm anomalies along the equatorial Pacific (Figure 6(c)). From Figures 5(d) and 6(c), it is apparent that warm (cold) ENSO years are associated with large (small) EPWP. It is also very interesting to note that the variability of the SST within the EPWP is comparatively very small. In other words, the variability of the EPWP arises from the changes in the area of the 28.5 °C isotherm and variations in the length of the EPWP season.

Table 3 shows the linear correlations amongst the variants (e.g. onset, demise, length, and seasonal area) of the EPWP. The onset date of the EPWP is significantly correlated with the length of the EPWP and the seasonal average of the area of the EPWP at −0.56 and −0.66, respectively. These linear correlations suggest that early (late) onset of the EPWP is associated with longer (shorter) EPWP season

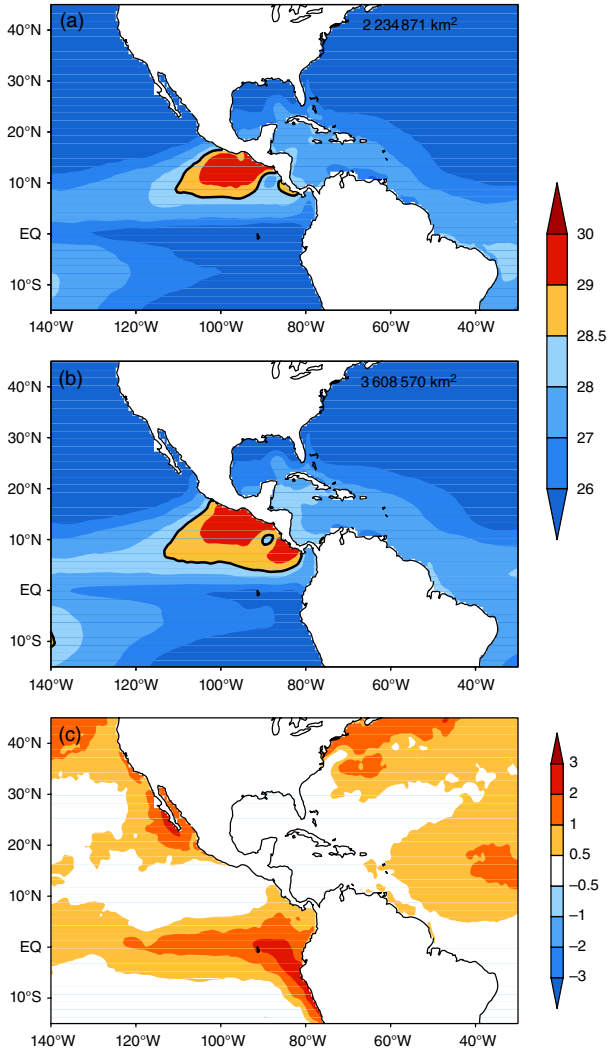

Figure 6. The composite seasonal mean of the SSTs (°C) for (a) bottom (small), (b) top (large) tercile (area of the EPWP), and (c) their difference (large - small). The composite area of the EPWP is indicated in the top right corner of (a) and (b).

and larger (smaller) seasonal mean area of the EPWP. The demise date of the EPWP, however, has a much stronger bearing on the length of the EPWP season with later (earlier) demise dates associated with longer (shorter) seasons (Table 3). Table 3 also shows that longer (shorter) seasons of EPWP season are also associated with the larger (smaller) seasonal mean area of the EPWP. It may be noted that the seasonal area of the EPWP is significantly

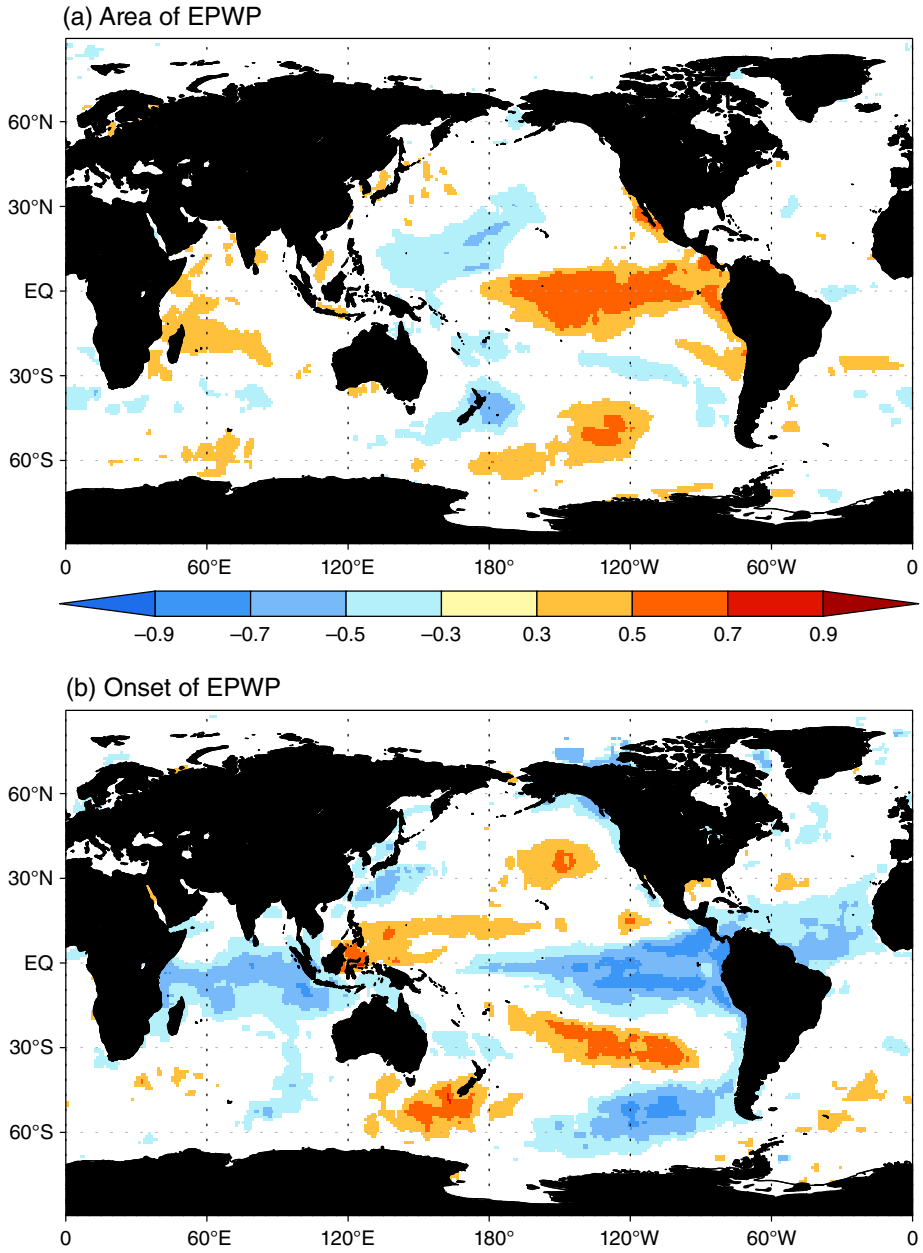

Figure 7. The correlation of the (a) April–May–June (AMJ) global SSTs with temporally coincident seasonal mean area of the EPWP and (b) leading January–February–March (JFM) global SSTs with onset date of the EPWP. Only significant correlations at 90% confidence interval are shown.

correlated with the onset date and length of the season but not with the demise date of the season.

In Figure 7(a), the association of the interannual variability of the seasonal area anomalies of the EPWP with ENSO variations in the eastern equatorial Pacific is clearly evident. The teleconnections of the area of the EPWP with positive correlations of AMJ SST anomalies over the north tropical Atlantic Ocean, tropical Indian Ocean and the horse-shoe pattern in the western Pacific Ocean that is associated with the ENSO variations are evident in Figure 7(a). In Figure 7(b), we see a similar SST pattern as Figure 7(a) with the onset date variations of the EPWP [but note that the global SST is from preceding January–February–March (JFM)] with the exception that the signs of the correlation are reversed. The teleconnections in Figure 7(b) suggest that the warm (cold) SST anomalies in JFM over the eastern equatorial Pacific Ocean, tropical Atlantic Ocean and the tropical Indian Ocean will lead to early (late) onset of the EPWP. Both these figures establish the well-known influence of ENSO on the EPWP (Wang and Enfield, 2003).

3.3. The relationship between EPWP and AWP

Since the EPWP occurs before the AWP forms in the Atlantic, it is worthwhile to examine their relationship. For example, the climatological onset and demise dates of the AWP are June 20 and November 4, respectively (Misra *et al.*, 2014). These dates occur

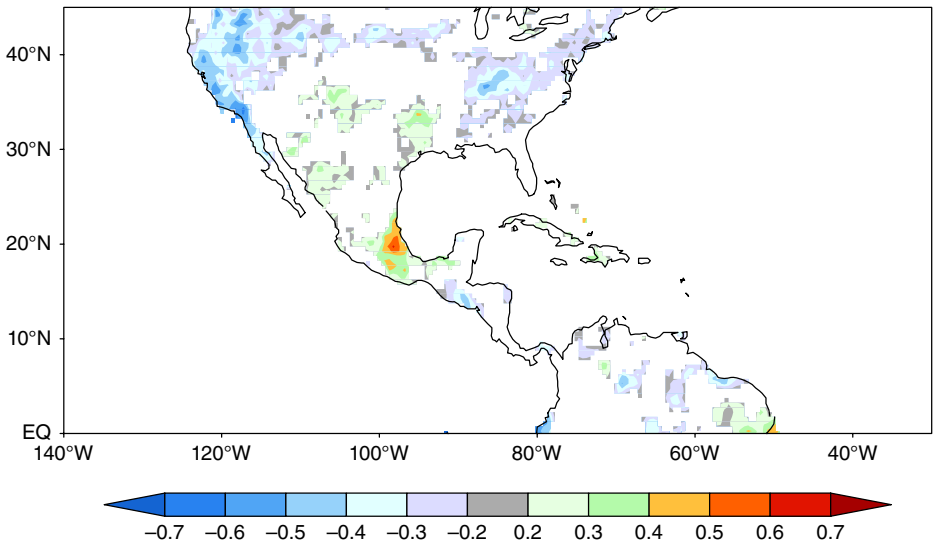

Figure 8. The correlation of the variability of the seasonal mean April–May–June (AMJ) rainfall with the onset of the EPWP season. Only significant values at 90% confidence interval are shaded.

much later than the corresponding climatological onset (March 22; Table 2) and demise (August 16; Table 2) dates of the EPWP. Table 4 shows the linear correlations between the variants of EPWP and AWP. Amongst the correlations shown in Table 4, the variations of the demise date and length of the EPWP season have statistically significant correlations with the corresponding variants of the AWP season. These correlations suggest that an early (late) demise date or shorter (longer) EPWP season is also likely to be associated with an early (late) demise date or shorter (longer) season of AWP. However, these correlations despite being statistically significant are relatively weak (in the range of 0.3–0.5). It is important to note that besides the demise date and length of the EPWP, all other variants of EPWP seem to have insignificant relationship with the AWP. In other words, these correlations reveal that the EPWP and AWP, despite being part of the WHWP, are quite independent of each other at least on interannual time scales. Lee *et al.* (2007) also arrived at a similar conclusion. This is consistent with the fact that the AWP variations (unlike the EPWP) are far more independent of ENSO variability and also exhibit significant internal variability associated with local air-sea, cloud-radiative feedbacks, and ocean heat transport through complex ocean current systems prevalent in the Intra-Americas Seas (Misra *et al.*, 2014 and references therein). More importantly, the AWP comprises nearly 80% of the WHWP (Wang and Enfield, 2003). Therefore, the EPWP by virtue of its size and its precedence by several months to the evolution of the seasonal peak of AWP will have far less influence on the latter.

3.4. The teleconnection of EPWP with continental rainfall over North America

The onset date of the EPWP shows some widespread correlations in Central America, southern Mexico, southwestern US, Pacific northwest and over Ohio valley (Figure 8). Figure 8 suggests that early (late) onset of the EPWP is likely to be associated with less (more) AMJ rainfall over Southeastern Mexico and Southwestern US (Pacific Northwest US and over Ohio valley). In a related observational study, KB9b show that ENSO modulation of EPWP SST leads to its strong influence on the Central American rainy season. In contrast, several other studies suggest that a SST gradient of warm Atlantic and cool equatorial Pacific conditions favour increased precipitation over the Caribbean region and Southern Mexico (Taylor *et al.*, 2002, 2011; Wang, 2007; Seager *et al.*, 2009; Fuentes-Franco *et al.*, 2014, 2015). In this study, we find that the EPWP variation as defined by the area of the 28.5 °C is unique from this trans-ocean SST anomaly gradients (Figure 7). In fact, KB9b argue that the impact of EPWP on Central American rainfall may have been underestimated because many of these studies considered Central America as part of a greater Caribbean region, thereby, implicitly assuming homogeneity across the region. Furthermore, we are examining the AMJ season, when the EPWP seasonal cycle peaks, unlike most other studies, which either examined the boreal summer and fall seasons or the annual mean anomalies.

Besides the feature of displaying robust interannual variability, the onset date of the EPWP can be used to assess the outlook of the forthcoming season based on some of these diagnosed teleconnection patterns. The remote teleconnections in Figure 8 can best be understood with the regression of the mean AMJ 500 hPa geopotential heights with the onset date of the EPWP (Figure 9(a)). These linear regressions show the weakening of the North Pacific High and general increase in the 500 hPa heights in the tropics with an early onset of EPWP, which is consistent with the atmospheric response to warm ENSO forcing (Wallace and Gutzler, 1981). Similarly, the regression of the mean AMJ 850 hPa winds with the onset date of the EPWP season shows that early (late) onset relates to weakening

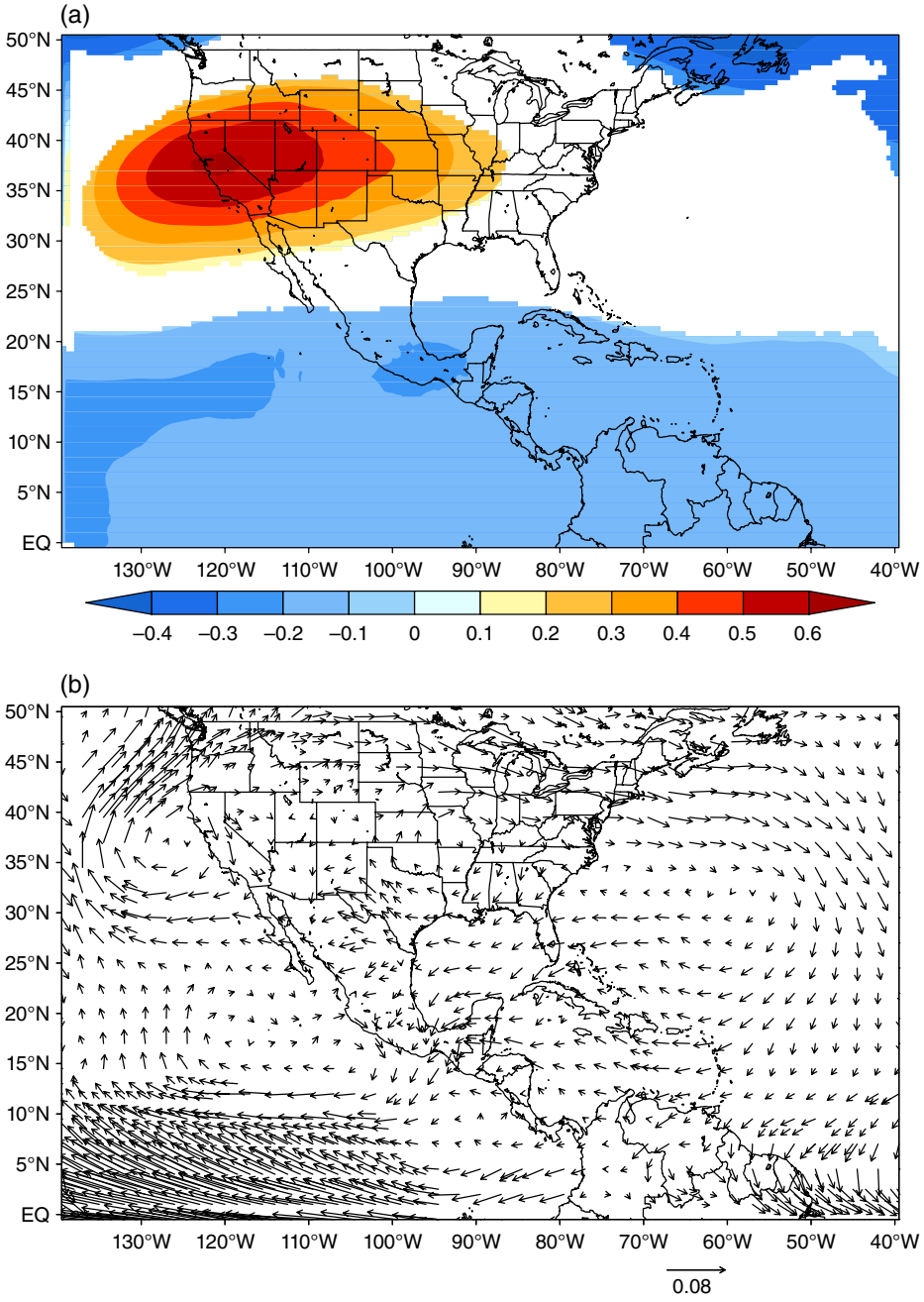

Figure 9. The regression of the (a) 500 hPa geopotential heights and (b) winds at 850 hPa with the onset date of the EPWP season. Only significant values at 90% confidence interval are shaded in (a) and are shown with bold arrows in (b).

(strengthening) of the easterlies (Figure 9(b)) that is akin to the ENSO modulation of the trade winds. Similarly, the correlation of the onset of the EPWP with the vertically integrated moisture flux convergence and regression of the vertically integrated moisture flux vectors with the onset date of the EPWP (Figure 10) are consistent with the teleconnections displayed in Figure 8. Figure 10 exhibits moisture flux divergence (convergence) over Southeastern Mexico, Southwestern US (Pacific Northwest US) with large (small) early (late) onset of the EPWP season in Figure 10(a) and (b). It may be noted that we did not find conclusive evidence to relate EPWP variations with the eastern Pacific tropical cyclone activity.

4. Summary and conclusions

The warm pool of the tropical northeast Pacific (EPWP) defined by the area enclosed by 28.5 °C SST isotherm exhibits a robust seasonal cycle. In this study, we have defined in an objective manner the onset, demise, and therefore the length of the EPWP season, which offers a novel way of examining the variability and seasonal evolution of the EPWP. The onset is defined as the day after the daily accumulated anomalies computed with respect to the climatological annual mean of the area of the EPWP reach a minimum. Similarly, the demise is defined as the day after the daily accumulated anomalies reach a maximum after the onset date is defined. In the case of the EPWP,

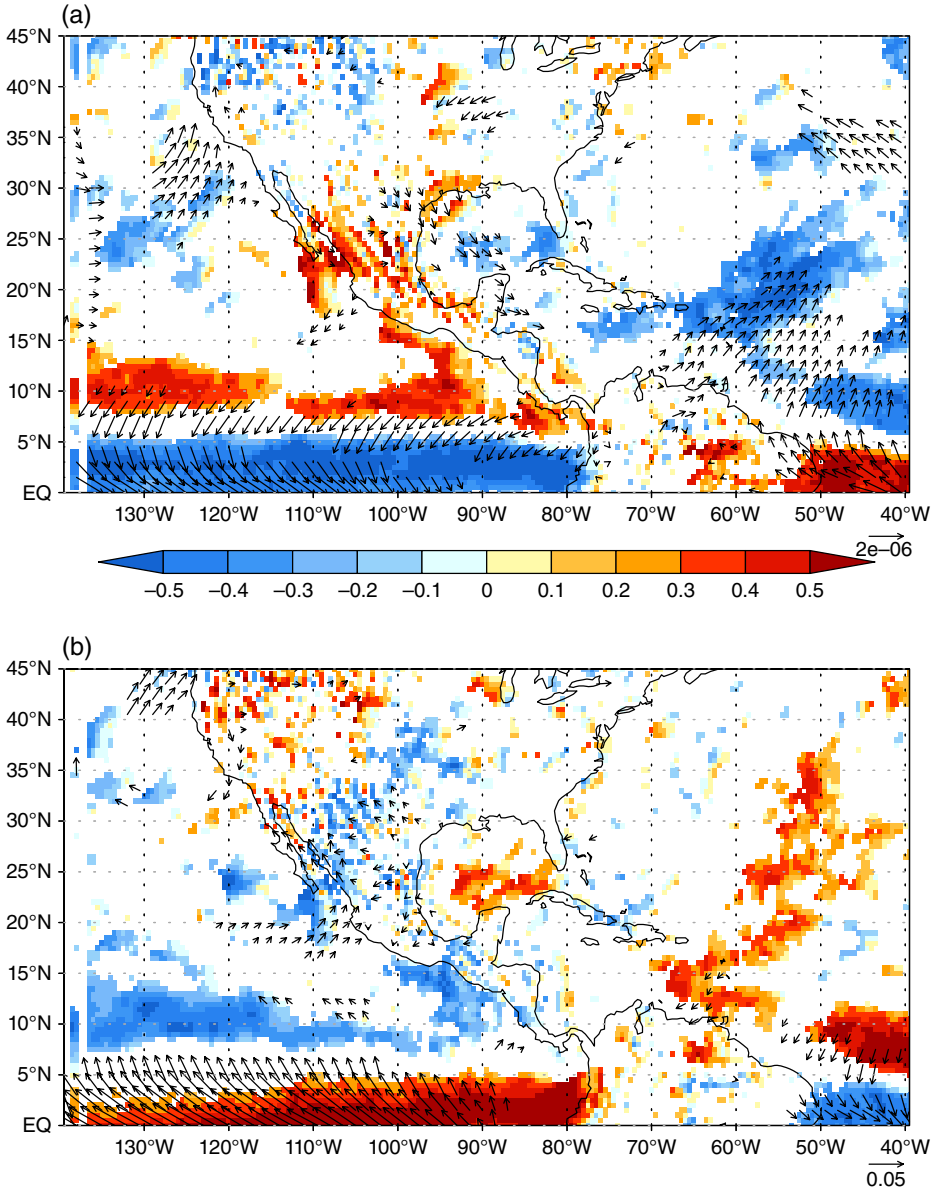

Figure 10. The correlation of the seasonal mean April–May–June (AMJ) anomalous moisture flux convergence and the regression of the vertically integrated moisture flux vectors regressed on (a) seasonal mean area of the EPWP and (b) onset date of the EPWP season. Only significant values at 90% confidence interval are plotted. The units for vectors in (a) is kg $s^{-1}m^{-1}$ km^{-2} and (b) kg $s^{-1}m^{-1}day^{-1}$.

these identified dates of onset (demise) coincide with the first (last) day of the daily anomalies of the area of the EPWP exceeding (reducing after onset) the climatological annual mean EPWP area. It is shown that the seasonal evolution of the EPWP is quite asymmetric with the seasonal peak occurring about 41 days from the onset date while the demise date occurs as late as 106 days after the seasonal peak. This asymmetry is also observed in the low-level wind confluence of the eastern Pacific ITCZ (Hastenrath, 2002). It is argued that such asymmetry in the EPWP seasonal cycle stems from the wind-evaporation SST feedback riding on the asymmetric meridional migration of the atmospheric ITCZ. The seasonal cycle of the surface fluxes also reveals that the downwelling shortwave flux dominates, followed by the latent heat flux over the EPWP region. The seasonal cycle of the surface fluxes reveals that the shortwave flux reaches a peak coinciding with EPWP seasonal cycle just as the latent heat flux is at its weakest part of the seasonal cycle.

The interannual variability of the EPWP coincides with ENSO variability. We find that the onset date variability of the EPWP season is closely related to the variability of the seasonal mean area of the EPWP season. For example, an early (late) onset of the EPWP season is likely to be associated with the large (small) seasonal mean area of the EPWP. ENSO has a stronger influence on the demise date variations of the EPWP than its onset date variations. Furthermore, the variations of the EPWP are characterized by rather weak SST variations within the 28.5 °C isotherm, which suggests that the variations largely stem from the variability of the area of the 28.5 °C isotherm and the length of the EPWP season.

The variations of the onset of the EPWP season are shown to have a significant relationship with variations of the subsequent AMJ seasonal mean continental rainfall variability over North America. These teleconnection patterns suggest that an early (late) onset of the EPWP is associated with less (more) AMJ rainfall over Southeastern Mexico and Southwestern US (Pacific Northwest US and over Ohio valley). These remote teleconnections are facilitated by the modulation of the large-scale circulation as observed in the modulation of the North Pacific High and the 500 hPa geopotential height patterns, which are very similar to the atmospheric response to ENSO forcing. We find that this teleconnection pattern is different from several other studies, which indicate the trans-basin (tropical Atlantic-equatorial eastern Pacific) SST anomaly gradient influencing the Central American rainfall. This could be reconciled by several factors including the fact that we show this relationship in the AMJ season, which coincides with the seasonal peak of EPWP.

This study reveals that the relationship between the EPWP and the AWP is weak even though they are both considered to be part of the WHWP. It may be noted that given the dominant intrinsic variations of AWP which are unrelated to ENSO, the small size of the EPWP relative to AWP, and the earlier seasonal peak of EPWP compared to AWP, are all likely the reasons for the weak relationship between the EPWP and the AWP. There are significant linear trends of the EPWP in the 35 years of the daily data that have been examined, which suggest increasing area, earlier onset and day of seasonal peak of EPWP in the last few decades. This has to be however further investigated in the context of global warming with longer observational records or mechanistic modelling studies.

Acknowledgements

This work was supported by grants from NOAA (NA12OAR4310078, NA10OAR4310215, NA11OAR 4310110) and USGS G13AC00408. The surface flux products were provided by the WHOI OAFlux project (http://oaflux.whoi.edu) funded by the NOAA Climate Observations and Monitoring (COM) program.

References

Amador JA, Alfaro EJ, Lizano OG, Magana VO. 2006. Atmospheric forcing of the eastern tropical Pacific: a review. *Progr. Oceanogr.* **69**: 101–142.

Banichevich A, Lizano OG. 1998. Interconexio´n a nivel ciclo´nico-atmosfe´rico entre el Caribe y el Pacı´fico. *Rev. Biol. Trop.* **46**(Suppl. 5): 9–21.

Chen M, Shi W, Xie P, Silva VBS, Kousky VE, Wayne Higgins R, Janowiak JE. 2008. Assessing objective techniques for gauge-based analyses of global daily precipitation. *J. Geophys. Res.* **113**: D04110, doi: 10.1029/2007 JD009132.

Crosbie E, Serra Y. 2015. Intraseasonal modulation of synoptic-scale disturbances and tropical cyclone genesis in the eastern North Pacific. *J. Clim.* **27**: 5724–5745.

Fiedler PC. 2002. The annual cycle and biological effects of the Costa Rica Dome. *Deep Sea Res.*, Part I **49**: 321–328.

Fuentes-Franco R, Coppola E, Giorgi F, Graef F, Pavia EG. 2014. Assessment of RegCM4 simulated inter-annual variability and daily-scale statistics of temperature and precipitation over Mexico. *Clim. Dyn.* **42**: 629–647, doi: 10.1007/s00382-013-1686-z.

Fuentes-Franco R, Coppola E, Giorgi F, Pavia EG, Diro GT, Graef F. 2015. Inter-annual variability of precipitation over Southern Mexico and Central America and its relationship to sea surface temperature from a set of future projections from CMIP5 GCMs and RegCM4 CORDEX simulations. *Clim. Dyn.* **45**: 425–440, doi: 10.1007/s00382-014-2258-6.

Hastenrath S. 2002. The intertropical convergence zone of the eastern Pacific revisited. *Int. J. Climatol.* **22**: 347–356.

Jien J, Gough W, Butler K. 2015. The influence of El Niño–Southern Oscillation on tropical cyclone activity in the Eastern North Pacific Basin. *J. Clim.* **28**(6): 2459–2474, doi: 10.1175/JCLI-D-14-00248.1.

Karnauskas KB, Busalacchi AJ. 2009a. Mechanisms for the interannual variability of SST in the East Pacific Warm Pool. *J. Clim.* **22**: 1375–1392, doi: 10.1175/2008JCLI2467.1.

Karnauskas KB, Busalacchi AJ. 2009b. The role of SST in the East Pacific Warm Pool in the interannual variability of Central American rainfall. *J. Clim.* **22**: 2605–2623, doi: 10.1175/2008JCLI2468.1.

Kessler WS. 2006. The circulation of the eastern tropical Pacific: a review. *Progr. Oceanogr.* **69**: 181–217.

Lee S-K, Enfield DB, Wang C. 2007. What drives the seasonal onset and decay of the Western Hemisphere warm pool? *J. Clim.* **20**: 2133–2146.

Liebmann B, Carmargo SJ, Seth A, Marengo JA, Carvalho LMV, Allured D, Fu R, Vera CS. 2007. Onset and end of the rainy season in South America in observations and the ECHAM 4.5 atmospheric general circulation model. *J. Clim.* **20**: 2037–2050.

Maloney ED, Hartmann DL. 2000. Modulation of eastern North Pacific hurricanes by the Madden–Julian oscillation. *J. Clim.* **13**: 1451–1460, doi: 10.1175/1520-0442(2000)013,1451:MOENPH.2.0.CO.

Minobe S. 1997. A 50–70 year climatic oscillation over the North Pacific and North America. *Geophys. Res. Lett.* **24**: 683–686.

Misra V, Li H, Kozar M. 2014. The precursors in the Intra-Americas seas to seasonal climate variations over North America. *J. Geophys. Res. (Oceans)* **119**(5): 2938–2948, doi: 10.1002/2014JC009911.

Mitchell TP, Wallace JM. 1992. The annual cycle in Equatorial convection and sea surface temperature. *J. Clim.* **5**: 1140–1156.

Raymond DJ, Raga GB, Bretherton CS, Molinari J, López-Carrillo C, Fuchs Ž. 2003. Convective forcing in the intertropical convergence zone of the east Pacific. *J. Atmos. Sci.* **60**: 2064–2082.

Raymond DJ, Esbensen SK, Paulson C, Gregg M, Bretherton CS, Petersen WA, Cifelli R, Shay LK, Ohlmann C, Zuidema P. 2004. EPIC2001 and the coupled ocean–atmosphere system of the tropical east Pacific. *Bull. Am. Meteorol. Soc.* **85**: 1341–1354, doi: 10.1175/BAMS-85-9-1341.

Reynolds RW, Smith TM, Liu C, Chelton DB, Casey KS, Schlax MG. 2007. Daily high-resolution-blended analyses for sea surface temperature. *J. Clim.* **20**: 5473–5496.

Ritchie EA, Wood KM, Gutzler DS, White SR. 2010. The influence of eastern Pacific tropical cyclone remnants on the southwestern United States. *Mon. Weather Rev.* **139**: 192–210.

Saha S, Moorthi S, Pan H-L, Wu X, Wang J, Nadiga S, Tripp P, Kistler R, Woollen J, Behringer D, Liu H, Stokes D, Grumbine R, Gayno G, Hou Y-T, Chuang H-Y, Juang H-MH, Sela J, Iredell M, Treadon R, Kleist D, van Delst P, Keyser D, Derber J, Ek M, Meng J, Wei H, Yang R, Lord S, van den Dool H, Kumar A, Wang W, Long C, Chelliah M, Xue Y, Huang B, Schemm J-K, Ebisuzaki W, Lin R, Xie P, Chen M, Zhou S, Higgins W, Zou C-Z, Liu Q, Chen Y, Han Y, Cucurull L, Reynolds RW, Rutledge G, Goldberg M. 2010. The NCEP climate forecast system reanalysis. *Bull. Am. Meteorol. Soc.* **91**: 1015–1057.

Seager R, Ting M, Davis M, Cane M, Naik N, Nakamura J, Li C, Cook E, Stahle DW. 2009. Mexican drought: an observational, modeling and tree ring study of variability and climate change. *Atmosfera* **22**: 1–31.

Small RJO, De Szoeke PS, Xie SP. 2007. The Central American Midsummer Drought: Regional Aspects and Large-Scale Forcing. *J. Clim.* **20**: 4853–4873.

Sneyers, R. 1990. On the statistical analysis of series of observations. WMO Technical note 143, WMO No. 415, TP-103, World Meteorological Organization, Geneva, Switzerland, 192 pp.

Taylor MA, Enfield DB, Chen AA. 2002. Influence of the tropical Atlantic versus the tropical Pacific on Caribbean rainfall. *J. Geophys. Res.* **107**(C9): 3127.

Taylor MA, Stephenson TS, Owino A, Chen AA, Campbell JD. 2011. Tropical gradient influences on Caribbean rainfall. *J. Geophys. Res.* **116**: D00Q08, doi: 10.1029/2010JD015580.

Wallace JM, Gutzler DS. 1981. Teleconnections in the geopotential height field during the Northern Hemisphere winter. *Mon.*

Weather Rev. **109**: 784–812, doi: 10.1175/1520-0493(1981)109<0784:TITGHF>2.0.CO;2.
Wang C. 2007. Variability of the Caribbean low-level jet and its relations to climate. *Clim. Dyn.* **29**: 411–422.
Wang C, Enfield DB. 2001. The tropical Western Hemisphere warm pool. *Geophys. Res. Lett.* **28**: 1635–1638.
Wang C, Enfield DB. 2003. A further study of the tropical Western Hemisphere warm pool. *J. Clim.* **16**: 1476–1493.
Wang C, Fiedler PC. 2006. ENSO variability in the eastern tropical Pacific: a review. *Progr. Oceanogr.* **69**: 239–266.
Wang C, Lee S-K, Enfield DB. 2007. Impact of the Atlantic warm pool on the summer climate of the Western Hemisphere. *J. Clim.* **20**: 5021–5040.
Willett CS, Leben R, Lavín MF. 2006. Eddies and mesoscale processes in the eastern tropical Pacific: a review. *Progr. Oceanogr.* **69**(2–4): 218–238.
Wood KM, Ritchie EA. 2013. An updated climatology of tropical cyclone impacts on the southwestern United States. *Mon. Weather Rev.* **141**: 4322–4336, doi: 10.1175/MWR-D-13-00078.1.
Wyrtki K. 1964. Upwelling in the Costa Rica Dome. *Fish. Bull.* **63**: 355–372.
Wyrtki K. 1965. Surface currents of the eastern tropical Pacific Ocean. *Inter-Am. Trop. Tuna Comm. Bull.* **9**: 271–304.
Wyrtki K. 1966. Oceanography of the eastern equatorial Pacific Ocean. *Oceanogr. Marine Biol. Annu. Rev.* **4**: 33–68.
Wyrtki K. 1967. Circulation and water masses in the eastern equatorial Pacific Ocean. *Int. J. Oceanol. Limnol.* **1**: 117–147.
Xie SP, Philander SGH. 1994. A coupled ocean-atmosphere model of relevance to the ITCZ in the eastern Pacific. *Tellus* **46A**: 340–350.
Xie SP, Xu H, Kessler WS, Nonaka M. 2005. Air-sea interaction over the eastern Pacific warm pool: gap winds, thermocline dome, and atmospheric convection. *J. Clim.* **18**: 5–20.
Yu L, Jin X, Weller RA. 2008. Multidecade global flux datasets from the Objectively analyzed Air-sea Fluxes (OAFlux) Project: latent and sensible heat fluxes, ocean evaporation, and related surface meteorological variables. OAFlux Project Technical Report OA-2008-01, Woods Hole Oceanographic Institution, Woods Hole, MA, 64 pp.
Zhang Y, Wallace JM, Battisti DS. 1997. ENSO-like interdecadal variability: 1900-93. *J. Clim.* **10**: 1004–1020.

